Simulation of electromechanical responses of ferroelectric ceramics driven by combined alternating electrical and mechanical loadings

Veng-cheong Lo,[a] Winnie Wing-yee Chung, and Simon Ching-kin Chow
Department of Applied Physics, The Hong Kong Polytechnic University, Hung Hom, Kowloon, Hong Kong, China

(Received 21 March 2007; accepted 15 April 2007; published online 15 June 2007)

The experimental result on dielectric and mechanical properties of $PbZr_xTi_{1-x}O_3$ driven by combined alternating electrical and mechanical loadings in various phase differences has been obtained by Zhou *et al.* [J. Appl. Phys. **96**, 6634 (2004)]. This paper presents the numerical simulation of this result using a two-dimensional four state Potts model. In this model, there are four different dipole orientations to reflect the coexistence of 90° and 180° domain walls. The coupling between the electrical and mechanical responses is implemented by the presence of two different ferroelastic strain states which are associated to the four different dipole orientations. The interactions of these dipoles and strains together with the mechanical energy density are incorporated into the system Hamiltonian. The enhanced and reduced electromechanical responses when the electric field and the compressive stress are out of phase and in phase, respectively, are reproduced by our model. © *2007 American Institute of Physics*. [DOI: 10.1063/1.2743819]

I. INTRODUCTION

The electromechanical property of ferroelectric materials is manifested by the presence of piezoelectricity and electrostriction, in which strain and polarization charge are induced by either electrical or mechanical stimuli or both. Perovskite-type ferroelectrics such as $PbZr_xTi_{1-x}O_3$ (PZT), $BaTiO_3$, and $Pb(Mg_{1/3}Nb_{2/3})O_3$-$PbTiO_3$ (PMN-PT) have been widely used for different types of electromechanical devices, because of their high speed, low power consumption, ability to be integrated with silicon integrated circuit, and high sensitivity. In the past, most of the applications essentially operate at high frequency and small amplitude.[1] Examples are ultrasonic generator, telephone diaphragm, and surface acoustic wave filter, etc. Under these conditions, linear constitutive relations are applicable to relate the stimuli (both mechanical and electrical) and the responses (both strain and polarization charge). Recently, low frequency and large amplitude applications are very common. Examples include the bending actuator for weaver's loom and noise control, piezomotor, and fuel injection valves for automobiles. For these applications, nonlinear relation exists between the responses and stimuli.[2]

There are many different combinations of applying external electromechanical loadings to the sample: (1) alternating electric field and static stress, (2) alternating stress and dc field, and (3) both alternating field and stress with different phase differences. It is worthwhile to investigate the electromechanical responses under different loading conditions. First of all, both the hysteresis loops of polarization versus electric field and strain versus electric field have been investigated under low frequency alternating electric field combined with a static uniaxial compressive stress.[2,3] Lynch.[4] and Zhou *et al.*[5] have shown that the remanent polarization decreases with the magnitude of the compressive stress. Moreover, the longitudinal strain ε_3 deceases with the compressive stress but the transverse strain ε_1 increases. On the other hand, for small compressive stress, the butterfly loop area increases with stress until the latter reaches a critical value. As the compressive stress further increases, the loop area is reduced and is finally constricted into a horizontal line. The reductions of remanent polarization and longitudinal strain can be explained by the suppression of the dipole alignment along the longitudinal direction in the presence of compressive stress. We have shown that the longitudinal compressive stress and transverse tensile stress play the equivalent role on the dipole orientations.[6,7] Similarly, both transverse compressive stress and longitudinal tensile stress enhance the ferroelectricity. The enlargement of the butterfly loop area upon the application of longitudinal compressive stress can be explained by the optimal 90° domain switching.[6] Under a small compressive stress, most of the dipoles are aligned along the transverse direction in the absence of electric field. Upon the application of the longitudinal electric field, dipoles rotate toward the longitudinal direction. This leads to a large number of dipoles undergoing 90° switching, as manifested by a large differential change in strain in the butterfly loop. If the magnitude of compressive stress is sufficiently large, all dipoles are clamped along the transverse direction. The application of electric field does not induce any dipole rotation. This results in a constricted butterfly loop (i.e., a horizontal line).

The electromechanical responses driven by an alternating stress under a dc electric bias have also been investigated.[3] Likewise, a family of stress-strain hysteresis curves under different electrical biasing conditions was obtained. The maximum dynamic strain was achieved when the dc biasing field ranges from 0.3 to 0.5 MV/mm. The previous interpretation for the existence of an optimal compres-

[a]Author to whom correspondence should be addressed; electronic mail: timothy.lo@polyu.edu.hk

sive stress to obtain a maximal dynamic strain response can also be used here. Again, 90° domain switching plays an important role.

The dielectric and piezoelectric responses of soft PZT under combined electric and mechanical loadings have been investigated by Zhou *et al.*[2] and Mitrovic *et al.*[8] These responses were dependent on the phase difference between the two loadings: in phase or out of phase. Even though the definitions on the phase difference are not the same, both of these authors observed enhanced electromechanical responses in one phase difference and reduced responses in the other. There has been so far no theoretical explanation nor any numerical simulation on this experimental result. In the paper, we present a theoretical explanation together with simulation for this result. The theoretical formulation is elaborated in the next section. Simulation results and discussion are presented in Sec. III.

II. THEORY AND MODELING

It has been mentioned before that the electromechanical responses are basically induced by 90° domain switching.[9,10] Any theory that intends to tackle the electromechanical problem should have the description on the 90° domain switching. The Landau theory with the two-dimensional geometry has been used before with both longitudinal and transverse polarization components.[11,12] However, there is no restriction on the relation between these two components to realize the 90° rotation. On the other hand, in the four-state Potts model, the existence of 90° domains can be modeled by the four mutually perpendicular states. The magnitude of the dipole moment for each of these states is constant. Consequently, we adopt the two-dimensional four-state Potts model. The details of this model have been described before.[6,13] The film is represented by the two-dimensional array of cells in xz plane. The size of the system is $N_x N_z$, where N_x and N_z are the numbers of cells along the x and z axes, respectively. The dipole at each cell is denoted by a pseudospin matrix $\hat{S}_{ij}$ which takes one of the four possible states (from a to d) as shown by the following expressions:

$$\begin{aligned}
&\hat{S}_{ij} = \hat{S}_a = \begin{pmatrix} 1 \\ 0 \end{pmatrix} \quad (\text{along} + z \text{ direction}),\\
&\hat{S}_{ij} = \hat{S}_b = \begin{pmatrix} 0 \\ 1 \end{pmatrix} \quad (\text{along} + x \text{ direction}),\\
&\hat{S}_{ij} = \hat{S}_c = \begin{pmatrix} -1 \\ 0 \end{pmatrix} \quad (\text{along} - z \text{ direction}), \quad \text{and}\\
&\hat{S}_{ij} = \hat{S}_d = \begin{pmatrix} 0 \\ -1 \end{pmatrix} \quad (\text{along} - x \text{ direction}),
\end{aligned} \tag{1}$$

where $0 < i \leqslant N_x$ and $0 < j \leqslant N_z$. The longitudinal direction is along the z axis, and the transverse direction is along the x axis. For a group of dipoles along the z axis (either in states a or c), a c domain is formed. Similarly, an a domain is formed for the aglomeration of dipoles in states b or d. To adopt the convention used by many authors in the literature, the components along z and x directions are labeled by "3" and "1," respectively.

The system Hamiltonian is given by

$$H = -\sum_{i,j,k,l} J\{\hat{S}_{ij}^T \hat{S}_{kl}\} - P_S \sum_{i,j} \{\hat{E}_{ij}^T \hat{S}_{ij}\} - \sum_{ij} \hat{\sigma}_{ij}^T \hat{\varepsilon}_{ij} - \alpha \sum_{i,j,k,l} \hat{\varepsilon}_{ij}^{F^T} \hat{\varepsilon}_{kl}^F + H', \tag{2}$$

where J is the coupling coefficient between neighboring dipoles, $\hat{X}^T$ is the transpose matrix of $\hat{X}$, the expression enclosed by the curly brace $\{\cdots\}$ denotes the matrix product, P_S is the saturation polarization, and α is the coupling coefficient between neighboring ferroelestic strain states. $\hat{E}_{ij}$, $\hat{\sigma}_{ij}$ and $\hat{\varepsilon}_{ij}$ are the matrix representations of electric field, stress, and strain, respectively. The subscripts i and j denote the location at the two-dimensional space, implying that these quantities are, in general, spatially inhomogeneous. Each of these matrices has the following generic form:

$$\hat{X} = \begin{pmatrix} X_3 \\ X_1 \end{pmatrix}. \tag{3}$$

On the right hand side of Eq. (3), the first row is the longitudinal component and the second transverse component. The last term in Eq. (2) caters for the anisotropic switching in which the change in the Hamiltonian for a 90° rotation of a longitudinal dipole is different from that of a transverse dipole, as has been discussed previously.[6] It can be explicitly expressed as

$$H' = -\sum_{ij} h_3(\phi_c - \phi_a)|\hat{n}^T \hat{S}_{ij}|, \tag{4}$$

where ϕ_c and $\phi_a = 1 - \phi_c$ are the probabilities of a dipole in c domain and a domain, respectively, h_3 is the energy barrier for switching a dipole from c to a domain, and $\hat{n}$ is a longitudinal unit matrix, given by $\hat{n} = \binom{1}{0}$.

The strain at each cell can be divided into three different contributions. (1) Ferroelastic strain $\hat{\varepsilon}_{ij}^F$ is associated with the dipole orientation and hence the pseudospin state as described before.[6,14,15,17] The two ferroelastic strain states are

$$\begin{aligned}
&\hat{\varepsilon}_{ij}^F = \hat{\varepsilon}_a = \begin{pmatrix} \varepsilon_0 \\ -\varepsilon_0/2 \end{pmatrix} \quad (\text{associated with the pseudospin states } a \text{ or } c), \quad \text{and}\\
&\hat{\varepsilon}_{ij}^F = \hat{\varepsilon}_b = \begin{pmatrix} -\varepsilon_0 \\ \varepsilon_0/2 \end{pmatrix} \quad (\text{associated with the pseudospin states } b \text{ or } d),
\end{aligned} \tag{5}$$

where ε_0 is the spontaneous strain of a tetragonal cell along the elongated edge. (2) Elastic strain $\hat{\varepsilon}_{ij}^{\text{el}}$ is a component that is due to the presence of stress wherein the material deforms elastically under a small stress or plastically for a stress exceeding the elastic limit. For a small stress, the relation between the strain and stress is linear, as described by the following equation:

$$\hat{\varepsilon}_{ij}^{\mathrm{el}} = \begin{pmatrix} \varepsilon_3^{\mathrm{el}} \\ \varepsilon_1^{\mathrm{el}} \end{pmatrix} = \frac{1}{Y} \begin{pmatrix} 1 & -\nu \\ -\nu & 1 \end{pmatrix} \begin{pmatrix} \sigma_3 \\ \sigma_1 \end{pmatrix}, \tag{6}$$

where Y and ν are, respectively, the Young's modulus and Poisson ratio. (3) Field-induced strain $\hat{\varepsilon}_{ij}^{\mathrm{EI}}$ is wherein the presence of electric field leads to the displacement of charges within a cell. It, in turn, creates distortion of the cell. Unlike the ferroelastic strain, this field-induced strain is not related to polarization switching (either by 180° flipping or 90° rotation). The relation of this strain with the electric field can be expressed as follows:[16]

$$\varepsilon_{mn} = d_{mnk}E_k + q_{mnkl}E_kE_l, \tag{7}$$

where d_{mnk} and q_{mnkl} are "piezoelectric" and "electrostriction" tensors, respectively; "m" is the direction of distortion and "n" is the normal of the cell surface. Thus, ε_{mm} is the normal strain and ε_{mn} is the shearing strain (for $m \neq n$). If we ignore the shearing strain, then we can merge the two indices into one, such that $\varepsilon_{mm}=\varepsilon_m$. The longitudinal and transverse components of the field-induced strain can then be expanded as follows:

$$\begin{aligned} (\varepsilon_3^{\mathrm{EI}})_{ij} &= d_{33}E_3 + d_{31}E_1 + q_{333}E_3^2 + q_{313}E_1E_3 + q_{331}E_3E_1 \\ &\quad + q_{311}E_1^2, \quad \text{and} \\ (\varepsilon_1^{\mathrm{EI}})_{ij} &= d_{13}E_3 + d_{11}E_1 + q_{133}E_3^2 + q_{113}E_1E_3 + q_{131}E_3E_1 \\ &\quad + q_{111}E_1^2. \end{aligned} \tag{8}$$

By the symmetry property, $d_{13}=d_{31}$, $q_{113}=q_{311}=q_{131}$, and $q_{313}=q_{133}=q_{331}$. Consequently, the total strain is the superposition of these three contributions, such that

$$\hat{\varepsilon}_{ij} = \hat{\varepsilon}_{ij}^{F} + \hat{\varepsilon}_{ij}^{\mathrm{el}} + \hat{\varepsilon}_{ij}^{\mathrm{EI}}. \tag{9}$$

The macroscopic quantities such as polarization and strains are calculated by the following relations:

$$P_3 = \frac{P_s \sum_{ij} \{\hat{n}^T \hat{S}_{ij}\}}{N_x N_z}, \tag{10}$$

$$\varepsilon_3 = \frac{1}{N_x N_z} \sum_{ij} \hat{n}^T (\hat{\varepsilon}_{ij} - \hat{\varepsilon}_{ij}^0), \tag{11}$$

and

$$\varepsilon_1 = \frac{1}{N_x N_z} \sum_{ij} \hat{q}^T (\hat{\varepsilon}_{ij} - \hat{\varepsilon}_{ij}^0), \tag{12}$$

where $\hat{\varepsilon}_{ij}^0$ is the initial strain matrix for each cell, and $\hat{q} = \binom{0}{1}$ is the transverse unit matrix.

The displacement vector can be evaluated by

$$D_3 = P_3 + \kappa_0 E_3, \tag{13}$$

where κ_0 is the permittivity in vacuum.

The system is initially unpoled and the initialization of the system of pseudospins has been discussed previously.[13] In order to simulate a film of finite thickness and of infinite width, free boundary condition is applied for both the top ($j=1$) and bottom ($j=N_z$) surfaces, and periodic boundary condition is adopted along the transverse direction. The film is subject to the alternating external electric field and stress which have the following common properties: (1) longitudinal, (2) triangular wave form, (3) of the same frequency, and (4) uniform in space. They can be expressed as follows:

$$\hat{E}(t) = \begin{pmatrix} E_0 \mathrm{Tri}(t,\Gamma,0) + E_{\mathrm{dc}} \\ E_1 \end{pmatrix}, \tag{14}$$

and

$$\hat{\sigma}(t) = \begin{pmatrix} \sigma_0 \mathrm{Tri}(t,\Gamma,\vartheta) + \sigma_{\mathrm{dc}} \\ \sigma_1 \end{pmatrix}, \tag{15}$$

where r_0 and r_{dc} are, respectively, the magnitude of the alternating loading and static component ($r=E$ and σ for electric field and stress, respectively); u_1 is the corresponding transverse component, t is time, Γ is the period, and ϑ is the phase difference between the two loadings. $\mathrm{Tri}(t,\Gamma,\vartheta)$ is the triangular wave function described as follows:

$$\mathrm{Tri}(t,\Gamma,\vartheta) = \begin{cases} u & 0 \leqslant u \leqslant 1 \\ 2-u & 1 \leqslant u \leqslant 3 \\ u-4 & 3 \leqslant u \leqslant 4 \end{cases} \tag{16}$$

where $u=4t'/\Gamma$, $t'=\mathrm{mod}[t+(\vartheta/2\pi)\Gamma,\Gamma]$, and $\mathrm{mod}(x,y)$ is the remainder function returning the remainder of the division of x/y. The Monte Carlo simulation does not involve time, so that both the period and the time should be scaled with the numbers of Monte Carlo steps (MSCs) according to the following relations:

$$\Gamma_{\mathrm{MCS}} = N_x N_z \frac{\Gamma}{\Delta t} \quad \text{and} \quad t_{\mathrm{MCS}} = N_x N_z \frac{t}{\Delta t}, \tag{17}$$

where Δt is the infinitesimal time step. The arguments on the left hand side of Eq. (17) are in unit of MCS.

Given the initial assembly of dipoles and strain states, their evolutions can be determined by the Metropolis algorithm. The macroscopic quantities at every instant are then evaluated according to Eqs. (11)–(13).

III. RESULTS AND DISCUSSION

The purpose of this work is to reproduce the experimental results obtained from Zhou and Kamlah[2] by numerical simulation. They applied alternating electrical and mechanical loadings on the PIC 151 piezoceramic sample. Both of these loadings are homogeneous and longitudinal. The transverse electric field component E_1 vanishes while there may be a nonzero transverse stress σ_1 due to the interaction between the sample and the electrode. Furthermore, we have adopted a sign convention that $\sigma>0$ for tensile stress and <0 for compressive stress. When $\vartheta=0°$, both the field and the stress reach their maximum values simultaneously (at point A) and then fall to their minima together (at point B). For $\vartheta=180°$, the field attains the maximum value while the stress value is minimum (at point A). Subsequently, the field arrives the minimum point when the stress is maximum (at point B). The timing diagrams of these loadings at difference phase relations are plotted in Fig. 1. Zhou *et al.*[2] have adopted another convention. They considered only the magnitude of the compressive stress. Consequently, their *in-*

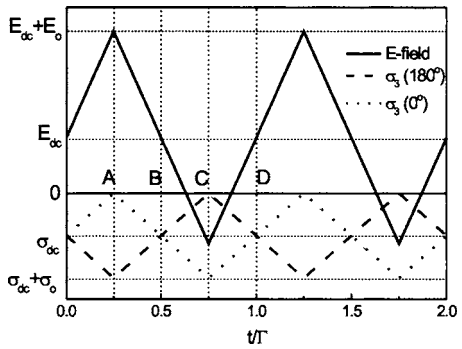

FIG. 1. The timing diagram of the external electric field (solid line) and compressive stresses at different phases: $\vartheta=180°$ (dash line) and $\vartheta=0°$ (dotted line). These phases angles correspond to the "in-phase" and "out-of-phase" conditions designated by Zhou *et al.*, respectively.

phase and *out-of-phase* conditions are equivalent to $\vartheta=180°$ and 0°, respectively, defined in our present paper. In the following discussion, in order to be consistent with the experimental results, we will use their convention.

The hysteresis loops of the displacement vector versus electric field (D_3-E_3) and strain versus electric field (ε_3-E_3) under different loading conditions are shown in Figs. 2 and 3, respectively. The simulation results are represented by lines in different types: solid line for out of phase, dotted line for in phase, and dashed lines for stress-free case, respectively. The experiments results are also shown on the same graphs by different symbols: solid squares, open squares, and open circles, respectively, for the corresponding loading conditions. We have chosen the following parameters for best-fitting the experimental results: the amplitude of alternating electric field $E_0=1.2$ kV/mm, period $\Gamma=60$ s, dc biased field $E_{dc}=0.8$ kV/mm, the amplitude of alternating compressive stress $\sigma_0=-12.5$ MPa, $\sigma_{dc}=12.5$ MPa, $\sigma_t=-3$ MPa, $J=1.29\times10^6$ J m^{-3}, $P_s=0.38$ C m^{-2}, $\varepsilon_0=2.5\times10^{-3}$, Young's modulus $Y=100$ GPa, Poisson ratio $\nu=0.3$, temperature $T=300$ K, $h_3=4.68\times10^5$ J m^{-3}, $\phi_C=0.45$, $d_{33}=250\times10^{-12}$ mV^{-1}, $d_{31}=-125$ mV^{-1}, $q_{113}=q_{311}=q_{131}=q_{313}=q_{133}=q_{331}\cong0$, $N_x=150$, and $N_z=80$.

From both the dielectric and mechanical responses, the out-of-phase condition yields the largest loop areas. The hysteretic loop under the in-phase condition is constricted nearly

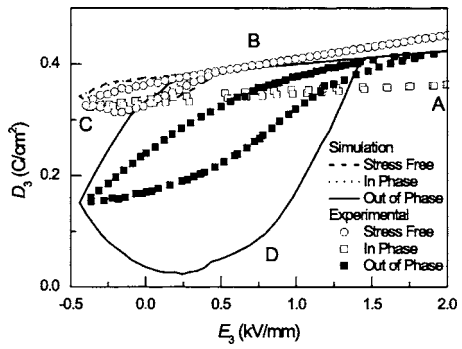

FIG. 2. Dielectric responses under different loading conditions. Simulation results are represented by a solid line (out of phase), a dotted line (in phase), and a dash line (stress-free). Experimental results are shown by solid squares (out of phase), open squares (in phase), and open circles (stress-free).

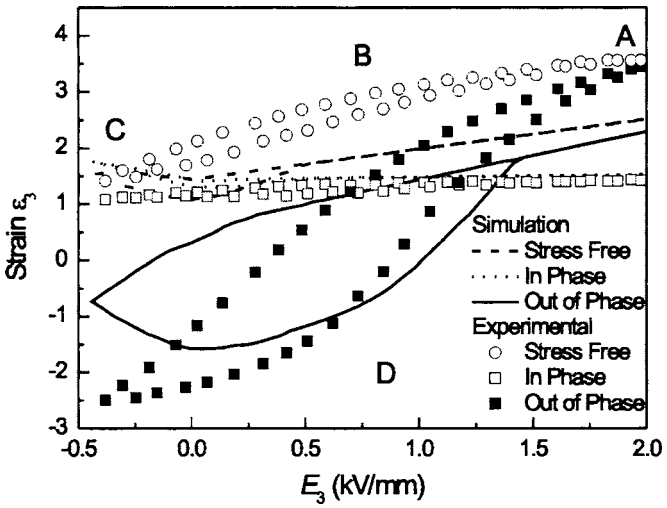

FIG. 3. Strain responses under different loading conditions. Simulation results are represented by a solid line (out of phase), a dotted line (in phase) and a dash line (stress-free). Experimental results are shown by solid squares (out of phase), open squares (in phase), and open circles (stress-free).

to a straight line. Moreover, regardless of the units, the profiles of both responses are quite similar under the identical loading condition. It has been well established that the strain response is caused by 90° domain switching through 90° rotation of dipoles near the domain walls.[18,19] The similarity between the dielectric and strain profiles in Figs. 2 and 3 reflects that the switching mechanism through 90° domain wall motions is also the dominant contribution of dielectric permittivity. There are two major types of contributions to the dielectric permittivity: intrinsic and extrinsic.[20] The former is due to the redistribution of charge clouds or the homogeneous deformation of a unit cell of ions in the presence of the driving field.[21] On the other hand, the latter is predominantly caused by domain wall switching: both 180° and 90° domains.[20,22] Xu *et al.*[20] suggested that significant non-180° domain wall switching occurs for a thin film with a thickness larger than 5 μm. Li *et al.*[22] attributed 60%–70% of the values of piezoelectric, dielectric, and elastic coefficients to the extrinsic contribution produced by non-180° domain wall movements. This explains the similarity in profiles for both dielectric and mechanical responses in Figs. 2 and 3.

Despite that Zhou *et al.* have given an explanation on the enhanced hysteresis loops for both dielectric and strain responses in the out-of-phase condition and the constricted loops in the in-phase case, how the microscopic picture on how each individual cell reacts at different times over a cycle has not been provided. We try to describe the responses of the dipole and the ferroelastic strain of a perovskite cell at the times labeled by points *A*, *B*, and *C* in Fig. 1. This description can illustrate different electromechanical responses under different phase relations. The in-phase condition is depicted in Fig. 4. Figure 4(a) corresponds to point *A* (Fig. 1), where both electric field and compressive stress are at their maximum values. The former encourages longitudinal dipole alignment, while the latter compels them along the transverse direction. These two influences cancel each other so that

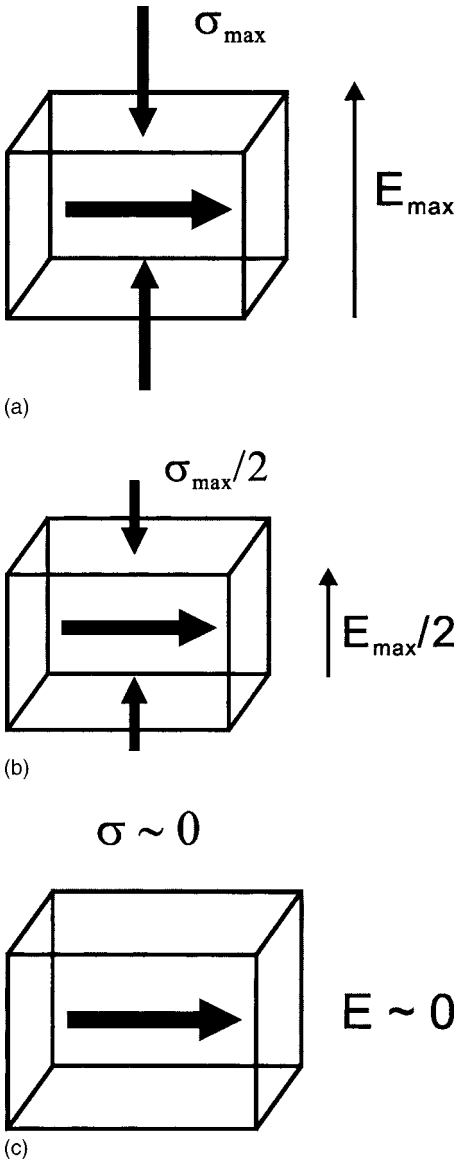

FIG. 4. Effect of alternating electric field and compressive stress on the dipole orientation and ferroelastic strain of a perovskite cell at different times under the in-phase condition: (a) point *A*, (b) point *B*, and (c) point *C*, corresponding to the timing diagram in Fig. 1.

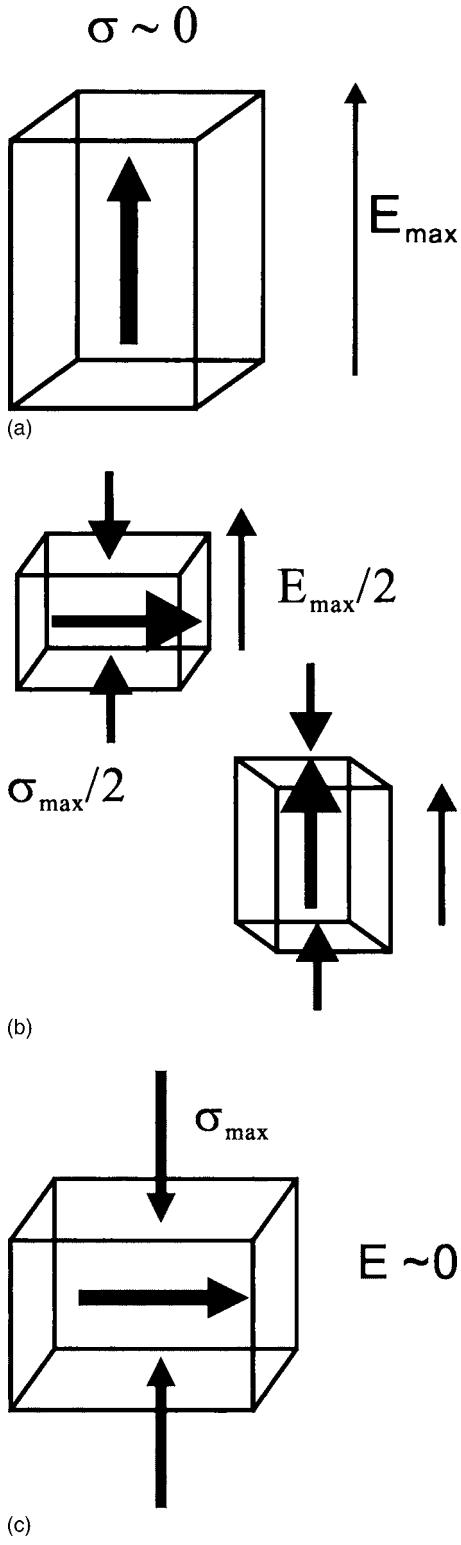

FIG. 5. Effect of alternating electric field and compressive stress on the dipole orientation and ferroelastic strain state of a perovskite cell at diffent times under the out-of-phase conditions: (a) point *A*, (b) point *B*, and (c) point *C*, corresponding to the timing diagram in Fig. 1.

there is no pronounced effect on the rotation of dipoles. In Fig. 4(b), corresponding to point *B* in Fig. 1, both the electric field and stress are reduced to one-half of their maximum values. Again, they cancel each other and there is no change on the dipole orientation. In Fig. 4(c), (point *C*), both influences are reduced to nearly zero. The dipole orientation remains unchanged in the absence of external influences. This leads to very small changes in the displacement and strain over a cycle, resulting in constricted hysteresis loops for both of them. On the other hand, in the out-of-phase case, the electric field is maximum while the compressive stress is absent, as shown in Fig. 5(a) (point *A*). The electric field drives a large amount of dipoles to the longitudinal direction. In Fig. 5(b) (point *B*), the field drops to one-half and the stress also increases to one-half of its maximum value. These two influences now cancel each other. A dipole may be aligned longitudinally or transversely, because some of them are thermally activated. Finally, in Fig. 5(c) (point *C*), the electric field drops to nearly zero while the compressive stress reaches the maximum. The compressive stress now becomes the dominant influence which forces the dipoles to be transversely aligned. Consequently, the dipole switches from state *a* to states *b* or *d* and then backs to state *a* again

over a cycle. This leads to tremendous changes in electric displacement and strain, resulting in enlarged hysteresis loops.

Comparing with the experimental results, our simulation successfully explains the effect of the phase difference on the electromechanical responses of a PZT ceramic sample. However, there is a discrepancy between the simulation and experimental results. The disagreement is obvious for the out-of-phase case where the hysteresis loops computed by simulation are larger than the experimental ones. There are a number of possibilities to account for this discrepancy. First of all, we have not considered the role of grain boundaries which are present in a polycrystalline ferroelectric sample. Many authors have proposed that domain wall motions are pinned by grain boundaries.[20,22,23] In particular, Xu *et al.*[20] have drawn this conclusion after studying the grain size effect on the electromechanical properties. Secondly, microcracks can be developed along the grain boundaries.[24] The field induced strains can be accommodated in microcracks.[25,26] Moreover, it has been reported that both the dielectric and mechanical properties are deteriorated by microcracks.[27,28] In our present model, we have not considered the presence of a space charge for simplicity.[29] The space charge effect should be present, especially at the head-to-head or tail-to-tail domain walls[28] where the discontinuity of polarization occurs. The presence of a space charge would induce an inhomogeneity of the electric field on one hand and depolarization on the other, even though it is not energetically favorable. Furthermore, its presence also leads to domain-wall pinning. Finally, the loop areas in Figs. 2 and 3 depend on how many dipoles that can be switched over a cycle. The switching anisotropy factor ϕ_c is an important parameter to reflect the preferential direction for the alignment of dipoles. If $\phi_c=1$, all dipoles in the sample are preferentially at states a or c (c domains). On a contrary, if $\phi_c=0$, they are in states b or d. It also manifests the inequality in probabilities of switching a dipole from c domain to a domain and vice versa.[6] The value of ϕ_c depends on the growth condition of the sample, the selection of substrate/electrode, as well as the built-in stress. For a large ϕ_c value, it is difficult to implement the 90° domain switching. As a result, the loop areas are constricted. In summary, the factors listed above can give rise to a hysteresis loop smaller than what we have obtained from simulation. To incorporate these effects would increase the complexity and computational cost.

In our description on the rotation of the dipole and hence the deformation of the cell in response to the external stress and field, we have assumed that there is no time delay between the responses and the stimuli. Practically, both the rotation of the dipole and the deformation of the cell to another pseudospin and strain state do not start immediately after the application of these stimuli. The factors responsible for this time delay are complicated. From both of our simulation and experimental results, the out-of-phase loading condition gives larger electromechanical responses (in terms of $\Delta\varepsilon_3$ and ΔD_3) than the in-phase case. Considering the time delay for the switching, it is expected that the optimal electromechanical responses might occur at a phase angle other than 0° or 180°. It deserves further experimental investigation to determine the optimal phase difference.

IV. CONCLUSION

In this work, the experimentally observed electromechanical responses under combined alternating electrical and mechanical loadings are numerically simulated using the four-state Potts model. In particular, both the strain-electric field and displacement hysteresis loops are more enlarged when both loadings are out of phase. They are constricted to straight lines when the loadings are in phase. The enhanced electromechanical responses can be explained by the pronounced 90° domain switching from which the electrical field and compressive stress take their roles at different times within a cycle.

ACKNOWLEDGMENT

This work is financially supported by the internal research grant from the Hong Kong Polytechnic University under Grant No. G-RGTC.

[1] K. Uchino, *Ferroelectric Devices* (Marcel Dekker, New York, 2000).
[2] D. Zhou and M. Kamlah, J. Appl. Phys. **96**, 6634 (2004).
[3] P. M. Chaplya and G. P. Carman, J. Appl. Phys. **90**, 5278 (2001).
[4] C. S. Lynch, Acta Mater. **44**, 4137 (1996).
[5] D. Zhou, M. Kamlah, and D. Munz, J. Mater. Res. **19**, 834 (2004).
[6] H.-x. Cao, V.-c. Lo, and W.-y. Chung, J. Appl. Phys. **99**, 024103 (2006).
[7] W. W.-y. Chung and V.-c. Lo, Mater. Res. Soc. Symp. Proc. **902E**, T10–51 (2006).
[8] M. Mitrovic, G. P. Carman, and F. K. Straub, Int. J. Solids Struct. **38**, 4357 (2001).
[9] V. Nagarajan, I. G. Jenkins, S. P. Alpay, H. Li, S. Aggarwal, L. Salamanca-Riba, A. L. Roytburd, and R. J. Ramesh, J. Appl. Phys. **86**, 595 (1999).
[10] K. Saito, T. Kurosawa, T. Akai, T. Oikawa, and H. Funakubo, J. Appl. Phys. **93**, 545 (2003).
[11] J. Zhang, Z. Yin, and M.-s. Zhang, Phys. Lett. A **310**, 479 (2003).
[12] H.-x. Cao, V.-c. Lo, and Z.-y. Li, J. Appl. Phys. **101**, 014113 (2007).
[13] K.-t. Li and V.-c. Lo, J. Appl. Phys. **97**, 034107 (2005).
[14] W. F. Li and G. J. Wang, J. Appl. Phys. **91**, 3806 (2002).
[15] B. Delibas, A. Arockiarajan, and W. Seemann, Mater. Sci. **16**, 507 (2005).
[16] B. A. Strukov and A. P. Levanyuk, *Ferroelectric Phenomena in Crytsals* (Springer-Verlag, Berlin, 1998).
[17] Y. F. Gao and Z. Suo, J. Appl. Mech. **69**, 419 (2002).
[18] V. Nagarajan, I. G. Jenkins, S. P. Alpay, H. Li, S. Aggarwal, L. Salamanca-Riba, A. L. Roytburd, and R. Ramesh, J. Appl. Phys. **86**, 595 (1999).
[19] C. S. Ganpule *et al.*, Appl. Phys. Lett. **77**, 292 (2000).
[20] F. Xu, S. Trolier-McKinstry, W. Ren, B. Xu, Z.-L. Xie, and K. J. Hemker, J. Appl. Phys. **89**, 1336 (2001).
[21] S. Li, W. Cao, and L. E. Cross, J. Appl. Phys. **69**, 7219 (1991).
[22] A. G. Luchaninov, A. V. Shil'Nikov, L. A. Shuvalov, and I. Ju. Shipkova, Ferroelectrics **98**, 123 (1989).
[23] A. H. Webster, T. B. Weston, and V. M. McNamara, J. Can. Ceram. Soc. **37**, 41 (1967).
[24] M. Takahashi, Jpn. J. Appl. Phys. **9**, 1236 (1970).
[25] X. Tan and J. K. Shangy, Philos. Mag. A **82**, 1463 (2002).
[26] J. Nuffer, D. C. Lupascu, A. Glazounov, H.-J. Kleebe, and J. Rödel, J. Eur. Ceram. Soc. **22**, 2133 (2002).
[27] C.-I. Cheon, S.-J. Kim, and H.-G. Kim, Ferroelectrics **115**, 34 (1991).
[28] T. Hauke, H. Beige, M. Giersbach, S. Seifert, and D. Sporn, Integr. Ferroelectr. **35**, 219 (2001).
[29] R. Ahluwalia and W. Cao, J. Appl. Phys. **89**, 8105 (2001).